ISSN 1070-3284, Russian Journal of Coordination Chemistry, 2022, Vol. 48, No. 5, pp. 325–331. © Pleiades Publishing, Ltd., 2022.

A Novel Tetrameric Heptomolybdate with Reactive Oxygen Species Catalytic Ability

J. A. Hua[a], X. Ma[a, *], J. Niu[b], B. X. Xia[a], X. Y. Gao[a], Y. L. Niu[b, **], and P. T. Ma[c, *]**

[a] *Chemistry and Chemical Engineering Department, Taiyuan Institute of Technology, Taiyuan, 030008 P.R. China*

[b] *Collaborative Innovation Center for CO_2 Conversion and Utilization, Taiyuan Institute of Technology, Taiyuan, 030008 P.R. China*

[c] *Henan Key Laboratory of Polyoxometalate Chemistry, College of Chemistry and Chemical Engineering, Henan University, Kaifeng, 475004 P.R. China*

**e-mail: maxiang@tit.edu.cn*

***e-mail: Niuyl@tit.edu.cn*

****e-mail: mpt@henu.edu.cn*

Received September 11, 2021; revised September 29, 2021; accepted September 30, 2021

Abstract—A novel polymolybdate based on tetrameric $\{Mo_7O_{24}\}$ cluster and copper complexes $[Na(H_2O)_7]_6[Cu(En)_2]_4\{[Na(H_2O)][H_{1.5}Mo_7O_{24}]\}_4\cdot 3H_2O$ (**I**, En = ethylenediamine) has been designed and characterized by IR spectrum, UV spectrum and single-crystal X-ray diffraction (CIF file CCDC no. 2104092). Structural data show that the main structure of **I** is a circular polyoxoanion that is alternately joined by $[Mo_7O_{24}]^{6-}$ clusters and sodium ions. The cations of **I** are in forms: $[Cu(En)_2]^{2+}$ and $[Na(H_2O)_7]^{+}$. Notably, **I** can efficiently catalyze the production of reactive oxygen species.

Keywords: tetrameric heptomolybdate, reactive oxygen species, catalytic ability, X-ray crystallography

DOI: 10.1134/S1070328422050050

INTRODUCTION

Reactive oxygen species (ROS), as the most common medium, is present in almost all pathological process [1, 2]. The researches of ROS catalyst have attracted increasing attention from the laboratory to the clinic [3–5]. In living organisms, Cu^{+}/Cu^{2+}, Fe^{2+}/Fe^{3+}, and Mn^{2+}/Mn^{4+} are used as active catalytic centers to construct reactive proteins that can produce ROS efficiently [6–8]. In recent years, several artificial enzyme based on polyoxometalate (POM) that can catalyze the production of ROS have been designed and synthesized [9–11], in which the catalytic activity of copper complexes is superior [12]. Hence, we will focus on composing the copper complexes with ROS catalytic activity.

POMs are a class of metal-oxygen clusters, which have multitudinous structures and fascinating properties in various fields [13–15]. POM have a number of inherent irreplaceable advantages, such as nano-size, nucleophilic oxygen-enriched surface, and polybond-making sites, which endow them to serve as bulky polydentate ligands with flexible coordination modes [16–24]. Among them, hitherto, investigations are mainly focused on heteropolyoxometalates (HTPs); in contrast, the reports on homopolyoxometalates (HMPs) are very limited although they are an important subfamily bearing enormous diversity of properties and structures [25, 26]. Moreover, it demonstrated that HMPs possessed an excellent oxidation catalytic capacity [27, 28], which may be beneficial to catalyze the production of ROS. Therefore, the combination of Cu complexes and HMPs in one hybrid structure may not only maintain the desirable properties of all precursor components, but also express them in a synergistic manner.

Herein we report a new designed HMP $[Na(H_2O)_7]_6[Cu(En)_2]_4\{[Na(H_2O)][H_{1.5}Mo_7O_{24}]\}_4\cdot 3H_2O$ (**I**, En is ethylenediamine), which was derived from tetrameric $\{Mo_7O_{24}\}$ cluster and $[Cu(En)_2]^{2+}$. As expected, complex **I** can catalyze ROS generation efficiently.

EXPERIMENTAL

Materials and methods. Reagents were all of analytical grade, purchased from commercial suppliers and used as received unless otherwise stated. $CuCl_2\cdot 2H_2O$, $Na_2MoO_4\cdot 2H_2O$, $(NH_4)_6Mo_7O_{24}\cdot 4H_2O$, and En were purchased from Macklin reagent Inc. (P.R. China). 2',7'-Dichlorofluorescin diacetate (DCFH-DA) was purchased from Sigma-Aldrich. All the solutions were prepared with Milli-Q water and filtered through a 0.22 μm filter (Millipore).

IR spectrum was obtained from a sample powder palletized with KBr on a Nicolet 170 SXFT-IR spectrophotometer over the range 4000–400 cm^{-1}. UV spectra were recorded on a UV-3600 spectrometer from 190 to 400 nm. DCF fluorescence were conducted on a Thermo Scientific Varioskan Flash microplate reader. Fluorescence spectra (λ_{ex} = 485 nm) from 505 to 650 nm were measured by a Varioskan Flash microplate reader (Thermo Scientific). C, H, and N elemental analyses were performed by using a PerkinElmer 2400-II CHNS/O analyzer. Inductively coupled plasma (ICP) spectra were obtained on a PerkinElmer Optima 2000 ICP-OES spectrometer.

Synthesis of $[Na(H_2O)_7]_6[Cu(En)_2]_4\{[Na(H_2O)][H_{1.5}Mo_7O_{24}]\}_4\cdot 3H_2O$ (I). A mixture of $Na_2MoO_4\cdot 2H_2O$ (0.70 g, 2.89 mmol), $(NH_4)_6Mo_7O_{24}\cdot 4H_2O$ (1.34 g, 5.00 mmol), $CuCl_2\cdot 2H_2O$ (0.17 g, 1.00 mmol), and En (0.2 mL) were dissolved in H_2O (20 mL) under stirring. The mixted suspension was keep in 85°C for 1.5 h and filtered when it was still hot. After 4 weeks, violet cuboid crystals of **I** were obtained in 22% yield (based on $CuCl_2\cdot 2H_2O$).

For $C_{16}H_{206}N_{16}O_{145}Na_{10}Cu_4Mo_{28}$					
Anal. calcd., %	C, 3.14	H, 3.34	N, 3.66	Mo, 43.93	Cu, 4.16
Found, %	C, 3.18	H, 3.33	N, 3.69	Mo, 44.33	Cu, 4.20

X-ray crystallography. A single crystal of **I** was mounted on a Bruker Apex-2 diffractometer with a CCD detector using graphite monochromatized MoK_α radiation (λ = 0.71073 Å) at 296 K. Data integration was performed using SAINT [29]. Routine Lorentz and polarization corrections were applied. Multiscan absorption corrections were performed using SADABS [30]. The remaining atoms were found from successive full-matrix least-squares refinements on F^2 and Fourier syntheses. All calculations were performed using the SHELXL-97 program package [31]. No hydrogen atoms associated with the water molecules were located from the difference Fourier map. Positions of the hydrogen atoms attached to the carbon and nitrogen atoms were geometrically placed. All hydrogen atoms were refined isotropically as a riding mode using the default SHELXTL parameters. A summary of crystal data and structure refinements for **I** is listed in Table 1.

Detailed information for structure **I** has been deposited with the Cambridge Crystallographic Data Centre (CCDC no. 2104092; deposit@ccdc.cam.ac.uk or http://www.ccdc.cam.ac.uk).

Catalytic ROS production of I. DCFH-DA stock solution (1 mM) was prepared with a buffer (20 mM Tris-HCl/150 mM NaCl, pH 7.4) according to the reported procedures [32]. Horseradish peroxidase (HRP) stock solution (4 μM) was prepared with the same buffer. Ascorbate (10 μM) without or with **I** (10 mg) were added to each sample and incubated at room temperature. The sample (200 μL) was transferred to the wells of a flat-bottomed 96-well black plate. HRP (0.04 μM) and DCFH-DA (100 μM) were added to each solution and incubated in the dark at room temperature for 12 h. The comparative groups, such as $(NH_4)_6Mo_7O_{24}\cdot 4H_2O$ (C1, 10 mg), $CuCl_2$ (Cu^{2+}, 0.25 mM), $CuCl_2$ + En (Cu^{2+} + En, 0.25 mM) and blank group, were also performed under the same conditions as described above.

RESULTS AND DISCUSSION

The structure of **I** was characterized by single-crystal X-ray diffraction analysis. The selected bond lengths and selected angles are summarized in Table S1 and Table S2, respectively. The unit of **I** consists of one $\{[Na(H_2O)]_4[Mo_7O_{24}]_4\}^{20-}$ polyanion, four $[Cu(En)_2]^{2+}$ and six $[Na(H_2O)_7]^+$ as counter cations, and three crystallization water. As shown in Fig. 1a, the polyoxoanion is constructed from four heptamolybdate $[Mo_7O_{24}]^{6-}$ and four $[Na(H_2O)]^+$, which are connected to each other forming a circular structure. The outer diameter of the circular structure is 18.96 Å and the inner diameter is 6.70 Å. As shown in Fig. 1b, the heptamolybdate $[Mo_7O_{24}]^{6-}$ is composed of two $\{Mo_2O_{10}\}$ clusters and one $\{Mo_3O_{14}\}$ cluster connected by edge sharing, which is different from the typical paramolybdate [33]. The typical configuration is planar, while the heptamolybdate $[Mo_7O_{24}]^{6-}$ in **I** is chair configuration as shown in Fig. 1c.

The bond valence sums (Σs) of atoms in **I** were further calculated according to the previous literature [34]. Briefly, the oxidation states of the atoms in **I** were calculated on the following formula:

$$V_i = \sum_j s_{ij} = \sum_j \exp\left(\frac{r_0' - r_{ij}}{B}\right),$$

which r_{ij} represents the observed values of bond distance that are listed in Table S1, and r_0' represents the theoretical value of bond distance between two atoms; B was set to 0.37 [35]. The theoretical values of Mo–O and Cu–N come from literatures, which the r_0' (Mo^{6+}–O) is 1.900 Å, and r_0' (Cu^{2+}–N) is 1.713 Å [35, 36]. As a results, the average valence state sums (Σs) of Mo and Cu ions in **I** are 6.121 and 1.943, which is basically consistent with the valence state of synthetic raw materials.

Based on the observed value of bond distance of **I**, the Σs can be calculated and the results are summarized in Table 2 and Fig. 2. The fragments of POM can easily been protonated, since they have high negative charges and rich basic surface oxygen atoms [37]. The

Table 1. Crystallographic data and structure refinements for **I**

Parameter	Value
Empirical formula	$C_{16}H_{206}N_{16}O_{145}Na_{10}Cu_4Mo_{28}$
Formula weight	6114.35
Crystal system	Orthorhombic
Space group	*Pnnm*
a, Å	13.659(4)
b, Å	23.022(7)
c, Å	26.812(8)
α, deg	90
β, deg	90
γ, deg	90
V, Å^3	8431(4)
Z	2
ρ_c, g cm^{-3}	2.409
μ, mm^{-1}	2.638
T, K	296(2)
Limiting indices	$-14 \le h \le 16$, $-27 \le k \le 26$, $-16 \le l \le 31$
Completeness to θ = 25.00, %	99.5
Measured reflections	31861
Independent reflections (R_{int})	7560 (0.0662)
GOOF on F^2	1.043
R indices ($I > 2\sigma(I)$)	$R_1{}^a = 0.0655$, $wR_2{}^b = 0.1817$
R indices (all data)	$R_1{}^a = 0.0975$, $wR_2{}^b = 0.2010$
$\rho\Delta_{max}/\rho\Delta_{min}$, e/A^3	1.748/−1.225

^{a} $R_1 = \Sigma\|F_o| - |F_c\|/\Sigma|F_o|$. ^{b} $wR_2 = |\Sigma w(|F_o|^2 - |F_c|^2)|/\Sigma|w(F_o)^2|^{1/2}$, where $w = 1/[\sigma^2(F_o^2) + (aP)^2 + bP]$. $P = (F_o^2 + 2F_c^2)/3$.

100 oxygen atoms in **I** can be classified into terminal O_t, bridging $O_{\mu2}$, $O_{\mu3}$ and $O_{\mu4}$. The O atoms with Σs of 0–1.65 could act as H-donors owing to the delocalized protons on them, whereas the O atoms with Σs of 1.90–2.00 possess dense electron cloud (see Table 2). In generally, the multiply protons usually assigned to be delocalized on the whole polyoxoanion, which the phenomenon is common in POM chemistry and has been reported in many leteratures, for example, $[Ni(EnMe)_2]_3[H_6Ni_{20}P_4W_{34}(OH)_4O_{136}(EnMe)_8(H_2O)_6]\cdot 12H_2O$ [34], $[Ni(En)_3]_2[H_2Nb_6O_{19}]\cdot 8H_2O$ [38], $[CuL(H_2O)][CuL]_2[P_2W_{18}O_{62}]\cdot 3H_2O$ [39], and $H_6[P_2Mo_5O_{23}]$ [40]. These results may indicate that the counter positive charges in **I** are delocalized in the $\{[Na(H_2O)]_4[Mo_7O_{24}]_4\}^{20-}$ skeleton, which may help to absorb protons and balance valence states of the system [41].

The IR spectrum of **I** shows similar the text asymmetric vibrations to other heptamolybdate $[Mo_7O_{24}]^{6-}$ containing species [33]. As shown in Fig. 3, three characteristic bands assigned to the ν(Mo–O_t), ν(Mo–$O_{\mu2}$), and ν(Mo–$O_{\mu3}$) appear at 890, 830, 629 cm^{-1}, respectively [33]. In addition, characteristic bands at 3316 cm^{-1} are ascribed to stretching vibrations of N–H which confirms the presence of En [42]. Vibration at 3425 cm^{-1} can be assigned to –OH stretch [43]. The IR spectrum is in good agreement with the result of X-ray diffraction structural analysis.

As shown in Fig. 4, the UV spectrum displays two absorption peaks in aqueous solution, which one centered at 206 nm and the other one with a wide shoulder absorption located at 228 nm in the region of 190–400 nm. These peaks may be assigned to $O_t \rightarrow Mo$ and $O_\mu \rightarrow Mo$ charge transfer transitions [37].

The influences of pH value on the stability of **I** have also been investigated by UV-Vis spectra. As shown in inset of Fig. 4, the UV-Vis absorption peaks of **I** showed no significant change between pH 5.05 and

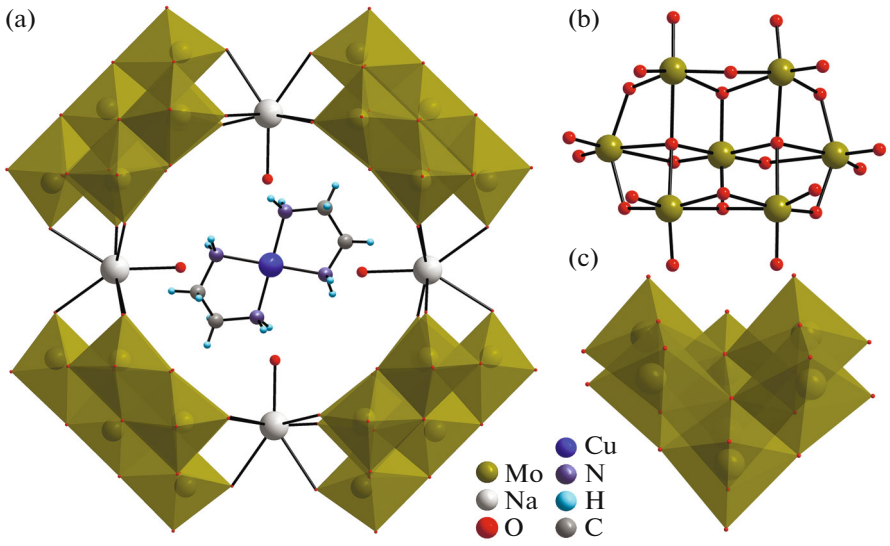

Fig. 1. Combined polyhedral/ball-and-stick representation of **I** (a); ball-and-stick view and polyhedral view of $[Mo_7O_{24}]^{6-}$ respectively (b and c). Lattice water molecules are omitted.

8.28 in intensity. Beyond the above pH range, absorption peaks at both 206 and 228 nm gradually changes in intensity, which may indicate that the skeleton of **I** began to collapse. Hence, the pH stability range of **I** is estimated to be in the range of 5.05 to 8.28.

Recently, we found that Cu complexes substituted POM possess the ability of catalytic oxidation [10]. The effect of **I** on the mediated ROS generation was thus investigated by dichlorofluorecin (DCF) assay. DCF is a fluorescent marker derived from the reaction of non-fluorescent 2',7'-dichlorofluorecin (DCFH)

Table 2. Bond valence and Σs of Mo, Cu in **I***

Bond	Valence	Bond	Valence	Bond	Valence	Atom	Σs
Mo(1)–O(1)	1.596	Mo(1)–O(1)$^{\#1}$	1.596	Mo(1)–O(8)	1.090		
Mo(1)–O(8)$^{\#1}$	1.090	Mo(1)–O(12)	0.379	Mo(1)–O(12)	0.379	Mo(1)	6.131
Mo(2)–O(4)	1.685	Mo(2)–O(2)	1.592	Mo(2)–O(10)	0.989		
Mo(2)–O(11)	0.976	Mo(2)–O(12)	0.505	Mo(2)–O(1)	0.186	Mo(2)	5.932
Mo(3)–O(3)	1.832	Mo(3)–O(7)	1.722	Mo(3)–O(9)	0.895		
Mo(3)–O(11)	0.834	Mo(3)–O(12)	0.449	Mo(3)–O(8)	0.414	Mo(3)	6.147
Mo(4)–O(6)	1.736	Mo(4)–O(5)	1.685	Mo(4)–O(9)	0.984		
Mo(4)–O(10)	0.757	Mo(4)–O(12)	0.544	Mo(4)–O(8)	0.375	Mo(4)	6.080
Mo(5)–O(13)	1.667	Mo(5)–O(14)	1.658	Mo(5)–O(22)	0.989		
Mo(5)–O(21)	0.984	Mo(5)–O(26)	0.485	Mo(5)–O(25)	0.214	Mo(5)	5.996
Mo(6)–O(16)	1.745	Mo(6)–O(15)	1.689	Mo(6)–O(17)	0.932		
Mo(6)–O(22)	0.857	Mo(6)–O(26)	0.489	Mo(6)–O(23)	0.385	Mo(6)	6.097
Mo(7)–O(25)	1.613	Mo(7)–O(24)	1.117	Mo(7)–O(23)	1.099		
Mo(7)–O(26)$^{\#2}$	0.412	Mo(7)–O(26)	0.412	Mo(7)–O(25)$^{\#2}$	1.613	Mo(7)	6.268
Mo(8)–O(18)	1.929	Mo(8)–O(19)	1.722	Mo(8)–O(20)	0.922		
Mo(8)–O(21)	0.864	Mo(8)–O(26)	0.502	Mo(8)–O(24)	0.379	Mo(8)	6.317
Cu(1)–N(1)	0.523	Cu(1)–N(2)	0.473	Cu(1)–N(3)	0.477		
Cu(1)–N(4)	0.470					Cu(1)	1.943

* Symmetry transformations used to generate equivalent atoms: $^{\#1}$ $-x, -y+1, z$; $^{\#2}$ $x, y, -z+1$.

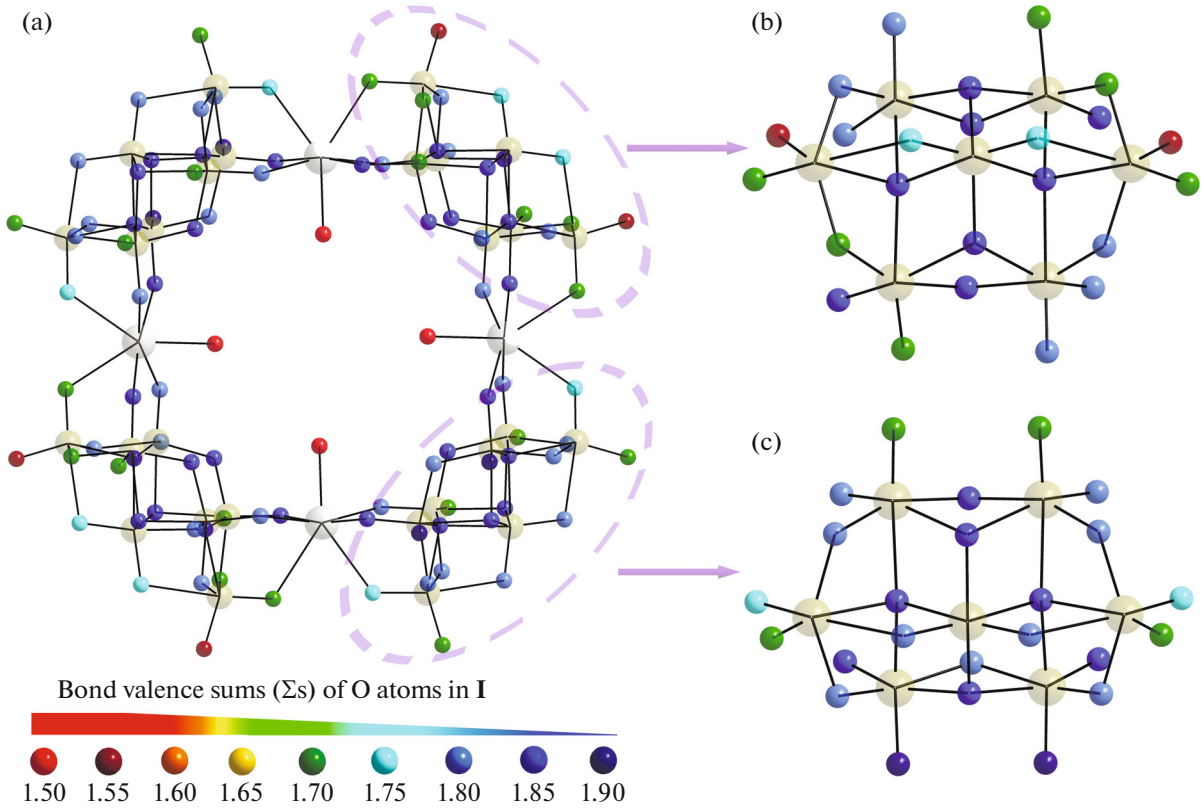

Fig. 2. Σs of oxygen atoms in the polyoxoanion of **I** (a) and heptamolybdate $[Mo_7O_{24}]^{6-}$ units (b and c). The extent of Σs for each oxygen atom is indicated by different colors.

reacted with ROS in the presence of horseradish peroxidase (HRP), which can indicate the total output of ROS from the system. As shown in Fig. 5, the fluorescence (λ_{em} = 528 nm) intensity of **I** group is obviously higher than that of blank group, which indicate that the production of ROS with **I** is more than that without it. Furthermore, $(NH_4)_6Mo_7O_{24}$ (abbreviated as C1) and $CuCl_2$ + En (abbreviated as Cu^{2+} + En) groups also have catalytic effects. However, the fluorescence intensity of **I** is about two fold higher than that of C1 and Cu^{2+} + En groups. Interestingly, the fluorescence intensity of Cu^{2+} group is lower than that of the blank group, which may indicate that the Cu^{2+} group produced significantly less ROS. This phenomenon may be original from the interaction between Cu^{2+} and HRP enzyme, which HRP can coordinate with Cu^{2+} making them lose their catalytic ability [44]. Hence, the combination of POM fragment and Cu-cluster may not only contribute to the synergistic production of ROS, but also protects the catalytic centers from interfering.

In this paper, a new tetrameric heptomolybdate $Na(H_2O)_7]_6[Cu(En)_2]_4\{[Na(H_2O)][H_{1.5}Mo_7O_{24}]\}_4 \cdot 3H_2O$ (**I**, En = ethylenediamine) has been designed and synthesized successfully. The novelty of the structure is that the $[Mo_7O_{24}]^{6-}$ clusters is alternately joined by $[Na(H_2O)]^+$ to forming a nanoscale circular cluster. Furthermore, **I** can efficiently catalyze the production of ROS, which may be due to the synergy effect of Cu complexes and POM fragments. The novelty structure and interesting property may make **I** a broad applica-

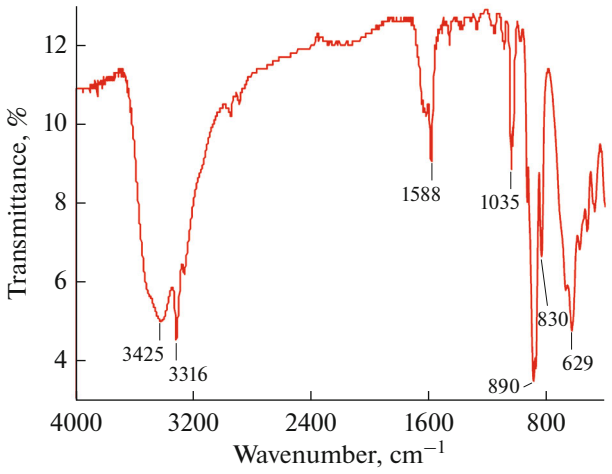

Fig. 3. IR spectrum for **I**.

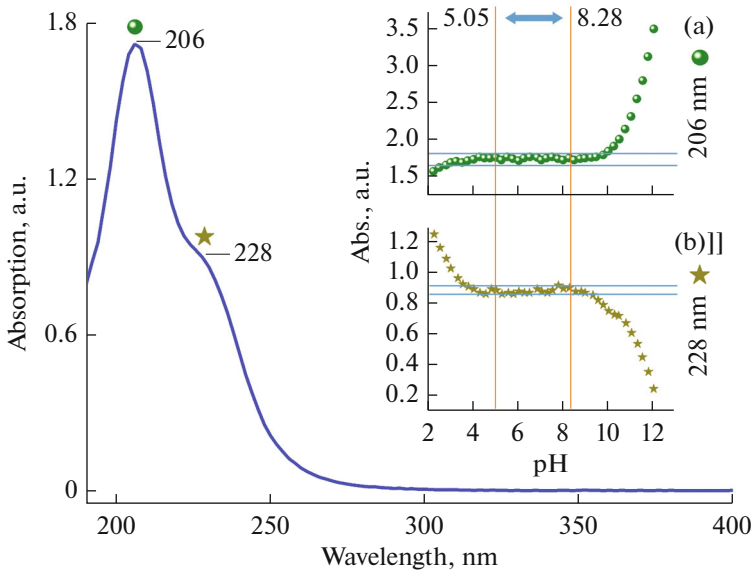

Fig. 4. UV-Vis spectra of **I** in ultrapure water and stability of **I** the range of pH (inset (a) and (b)).

tion prospects in the biochemistry and inorganic chemistry researches of ROS catalyst.

FUNDING

This work was supported by the Shanxi Province Science Foundation for Youths (Grants 201901D211453 and 20210302124333), the Fund for Shanxi "1331" Project, and the Scientific and Technological Innovation Programs of Higher Education Institutions in Shanxi (STIP 2020L0643 and 2020L0644).

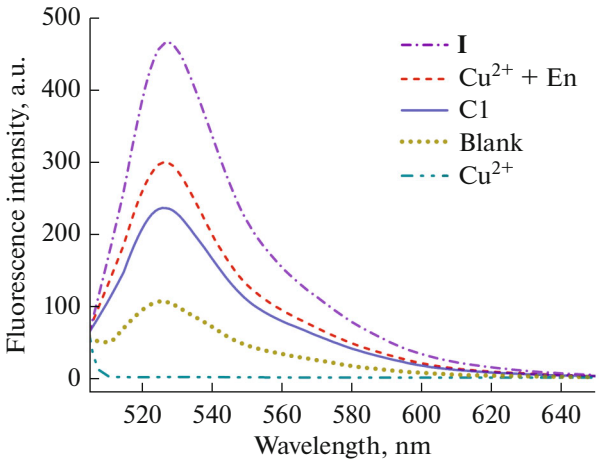

Fig. 5. Fluorescence intensity of DCF (λ_{ex} = 485 nm) in Tris-buffer (20 mM Tris-HCl/150 mM NaCl, pH 7.4) induced by **I** (10 mg), $(NH_4)_6Mo_7O_{24}\cdot 4H_2O$ (C1, 10 mg), $CuCl_2$ (Cu^{2+}, 0.25 mM), $CuCl_2$ + En (Cu^{2+} + En, 0.25 mM) groups and control group.

CONFLICT OF INTERESTS

The authors declare that they have no conflicts of interest.

AUTHOR CONTRIBUTIONS

X. Ma and J.A. Hua conceived the idea of the research, X. Ma and J.A. Hua designed the molecule, and J.A. Hua and J. Niu synthesized the molecule. X. Ma, B.X. Xia, and X.Y. Gao designed and conducted the experiments. J.A. Hua, Y.L. Niu, and P.T. Ma analyzed the data. All authors wrote and reviewed the manuscript.

SUPPLEMENTARY INFORMATION

The online version contains supplementary material available at https://doi.org/10.1134/S1070328422050050.

REFERENCES

1. Kepp, K.P., *Chem. Rev.*, 2012, vol. 112, p. 5193.
2. Zhou, Z.J., Song, J.B., Nie, L.M., and Chen, X.Y., *Chem. Soc. Rev.*, 2016, vol. 45, p. 6597.
3. Jiang, D.W., Ni, D.L., Rosenkrans, Z.T., et al., *Chem. Soc. Rev.*, 2019, vol. 48, p. 3683.
4. Shahidi, F. and Zhong, Y., *Chem. Soc. Rev.*, 2010, vol. 39, p. 4067.
5. Yao, Y.J., Zhang, H.L., Wang, Z.Y., et al., *J. Mater. Chem. B*, 2019, vol. 7, p. 5019.
6. Dickinson, L.C. and Symons, M.C.R., *Chem. Soc. Rev.*, 1983, vol. 12, p. 387.
7. Xu, L.H., Ji, X.H., Zhao, N., et al., *Polym. Chem.*, 2016, vol. 7, p. 1826.
8. Mishra, P., Satpati, S., Baral, S.K., et al., *Mol. Biosyst.*, 2016, vol. 12, p. 3017.

9. Ma, X., Zhou, F.T., Yue, H., et al., *J. Mol. Struct.*, 2019, vol. 1198, p. 126865.
10. Ma, X., Zhang, C., Hua, J.A., et al., *CrystEngComm*, 2019, vol. 21, p. 394.
11. Ma, X., Zhao, Q., Wang, B., et al., *J. Mol. Struct.*, 2020, vol. 1206, p. 127714.
12. Hua, J.A., Yuan, X., Ma, X., et al., *CrystEngComm*, 2020, vol. 22, p. 7832.
13. Du, D.Y., Qin, J.S., Li, S.L., et al., *Chem. Soc. Rev.*, 2014, vol. 43, p. 4615.
14. Adonin, S.A., Peresypkina, E.V., Sokolov, M.N., et al., *Inorg. Chem.*, 2014, vol. 53, p. 6886.
15. Moussawi, M.A., Leclerc-Laronze, N., Floquet, S., et al., *J. Am. Chem. Soc.*, 2017, vol. 139, p. 12793.
16. Banerjee, A., Bassil, B.S., Roschenthaler, G.V., and Kortz, U., *Chem. Soc. Rev.*, 2012, vol. 41, p. 7590.
17. Mukhacheva, A.A., Volchek, V.V., Yanshole, V.V., et al., *Inorg. Chem.*, 2020, vol. 59, p. 2116.
18. Jin, H.J., Zhou, B.B., Yu, Y., et al., *CrystEngComm*, 2011, vol. 13, p. 585.
19. Arnau del Valle, C., Felip-Leon, C., Angulo-Pachon, C.A., et al., *Inorg. Chem.*, 2019, vol. 58, p. 8900.
20. Meng, J.X., Lu, Y., Li, Y.G., et al., *CrystEngComm*, 2011, vol. 13, p. 2479.
21. Xu, X.X., Gao, X., Lu, T.T., et al., *J. Mater. Chem. A*, 2015, vol. 3, p. 198.
22. Feng, S.L., Lu, Y., and Zhang, Y.X., *Dalton Trans.*, 2018, vol. 47, p. 14060.
23. Ma, Y., Xue, Q., Min, S.T., et al., *Dalton Trans.*, 2013, vol. 42, p. 3410.
24. Li, F.Y. and Xu, L., *Dalton Trans.*, 2011, vol. 40, p. 4024.
25. Chen, X.X., Wang, Z., Zhang, R.R., et al., *Chem. Commun.*, 2017, vol. 53, p. 10560.
26. Chupina, A.V., Mukhacheva, A.A., Abramov, P.A., and Sokolov, M.N., *J. Struct. Chem.*, 2020, vol. 61, p. 299.
27. Maksimchuk, N.V., Evtushok, V.Y., Zalomaeva, O.V., et al., *ACS Catal.*, 2021, vol. 11, p. 10589.
28. Zhang, S.W., Ou, F.X., Ning, S.G., and Cheng, P., *Inorg. Chem. Front.*, 2021, vol. 8, 1865.
29. *SAINT*, Madison (WI, USA): Bruker AXS Inc., 2007.
30. Brese, N.E. and O'Keeffe, M., *Acta Crystallogr., Sect. B: Struct. Sci.*, 1991, vol. 47, p. 192.
31. Sheldrick, G.M., *SHEXTL-97, Programs for Crystal Structure Refinements,* Göttingen: Univ. of Göttingen, 1997.
32. Ma, X., Wang, Y.Q., Hua, J.A., et al., *Sci. China Chem.*, 2020, vol. 63, p. 73.
33. Li, J., Liu, Y., Luo, J., et al., *Russ. J. Coord. Chem.*, 2011, vol. 37, p. 849. https://doi.org/10.1134/S107032841110006X
34. Zheng, S.T., Zhang, J., Juan, J.M., et al., *Angew. Chem. Int. Ed. Engl.*, 2009, vol. 48, p. 7176.
35. Brown, I.D. and Altermatt, D., *Acta Crystallogr., Sect. B: Struct. Sci.*, 1985, vol. 41, p. 244.
36. Shields, G.P., Raithby, P.R., Allen, F.H., and Motherwell, W.D.S., *Acta Crystallogr., Sect. B: Struct. Sci.*, 2000, vol. 56, p. 455.
37. Ma, X., Hua, J.A., Wang, K., et al., *Inorg. Chem.*, 2018, vol. 57, p. 13533.
38. Ma, X., Bian, Y.J., Zhou, Y.J., et al., *J. Clust. Sci.*, 2021, vol. 32, p. 613.
39. Ma, X., Zhou, Y.J., Yuan, X.R., et al., *Inorg. and Nano-Met. Chem.*, 2021, vol. 51, p. 332.
40. Hua, J.A., Tian, Y., Bian, Y.J., et al., *SN Appl. Sci.*, 2020, vol. 2, p. 308.
41. Rausch, B., Symes, M.D., and Cronin, L., *Chem. Commun.*, 2018, vol. 54, p. 1093.
42. Hua, J.A., Zhou, Y.J., Bian, Y.J., et al., *J. Coord. Chem.*, 2020, vol. 73, p. 282.
43. Hua, J.A., Duan, Z.P., Gao, C.K., et al., *Russ. J. Coord. Chem.*, 2021, vol. 47, p. 646. https://doi.org/10.1134/S1070328421090049
44. Zhao, J.S., Wang, Y., Zhou, J.W., et al., *J. Mater. Chem., A*, 2016, vol. 4, p. 7174.